Inorg. Chem. **2003**, *42*, 5282–5292

Synthesis, Characterization, and Computational Study of the *trans*-$IO_2F_5^{2-}$ Anion

Jerry A. Boatz,[†] Karl O. Christe,*[,†,‡] David A. Dixon,[§] Barbara A. Fir,[||] Michael Gerken,[||,⊥] Robert Z. Gnann,[‡] Hélène P. A. Mercier,[||] and Gary J. Schrobilgen*[,||]

Loker Hydrocarbon Research Institute, University of Southern California, University Park, Los Angeles, California 90089, Air Force Research Laboratory, Edwards Air Force Base, California 93524, Department of Chemistry, McMaster University, Hamilton, Ontario L8S 4M1, Canada, and The Fundamental Sciences Division, Pacific Northwest National Laboratory, Richland, Washington 99352

Received April 30, 2003

The combination of CH_3CN solutions of $[N(CH_3)_4][F]$ and a mixture of *cis*- and *trans*-$[N(CH_3)_4][IO_2F_4]$ produces the novel *trans*-$IO_2F_5^{2-}$ anion. Under the given conditions, only the *trans*-$IO_2F_4^-$ anion acts as a fluoride ion acceptor, thus allowing the separation of isomerically pure, soluble *cis*-$IO_2F_4^-$ from insoluble *trans*-$IO_2F_5^{2-}$. The *trans*-$IO_2F_5^{2-}$ and *cis*-$IO_2F_4^-$ anions were characterized by infrared and Raman spectroscopy and theoretical calculations at the LDFT and HF levels of theory. The *trans*-$IO_2F_5^{2-}$ anion has a pentagonal-bipyramidal geometry with the two oxygen atoms occupying the axial positions. It represents the first example of a heptacoordinated main group AO_2X_5 species and completes the series of pentagonal-bipyramidal iodine fluoride and oxide fluoride species. The geometries of the pentagonal-bipyramidal series $IO_2F_5^{2-}$, IOF_5^{2-}, IF_5^{2-}, IOF_6^-, IF_6^-, and IF_7 and the corresponding octahedral series $IO_2F_4^-$, IOF_4^-, IF_4^-, IOF_5, IF_5, and IF_6^+ were calculated by identical methods. It is shown how the ionic charge, the oxidation state of the iodine atom, the coordination number, and the replacement of fluorine ligands by either an oxygen ligand or a free valence electron pair influence the stuctures and bonding of these species.

Introduction

Main-group fluorides and oxofluorides offer a unique opportunity to study high coordination numbers, the steric influence and relative repulsive effects of fluorine, oxygen and sterically active free valence electron pairs, and fluxionality. Of particular interest in this respect is the coordination number 7. Although heptacoordinated species can exist in three different conformations of similar energy, i.e., either as a monocapped octahedron, a monocapped trigonal prism, or a pentagonal bipyramid,[1,2] main-group elements generally prefer pentagonal-bipyramidal structures[3,4] because this geometry results in a better overlap of the ligand orbitals with the s and p orbitals of the central atom (A). As part of our systematic studies of heptacoordination, the structures of main-group AF_5XY species have been studied where X and Y represent either fluorine or oxygen ligands or sterically active free valence electron pairs (E).[3,5−14] Structures for all

* To whom correspondence should be addressed. E-mail: karl.christe@edwards.af.mil (K.O.C.); schrobil@mcmaster.ca (G.J.S.).
† Air Force Research Laboratory.
‡ Loker Hydrocarbon Research Institute.
§ Pacific Northwest National Laboratory. E-mail: david.dixon@pnl.gov.
|| McMaster University.
⊥ Present address: Department of Chemistry and Biochemistry, The University of Lethbridge, Lethbridge, Alberta T1K 3M4, Canada. E-mail: michael.gerken@uleth.ca.

(1) Kepert, D. L. *Inorganic Stereochemistry*; Springer-Verlag: Heidelberg, Germany, 1981.
(2) (a) Gillespie, R. J.; Hargittai, I. *The VSEPR Model of Molecular Geometry*; Allyn and Bacon, A Division of Simon & Schuster, Inc.: Needham Heights, MA, 1991. (b) Gillespie, R. J.; Popelier, P. L. A. *Chemical Bonding and Molecular Geometry: from Lewis to Electron Densities*; Oxford University Press: New York, 2001.
(3) Christe, K. O.; Curtis, E. C.; Dixon, D. A.; Mercier, H. P. A.; Sanders, J. C. P.; Schrobilgen, G. J.; Wilson, W. W. *Inorganic Fluorine Chemistry Toward the 21st Century*; Thrasher, J. S., Strauss, S. H., Eds.; ACS Symposium Series 555; American Chemical Society: Washington, DC, 1994; Chapter 5, pp 66−89.
(4) Seppelt, K. *Inorganic Fluorine Chemistry Toward the 21st Century*; Thrasher, J. S., Strauss, S. H., Eds.; ACS Symposium Series 555; American Chemical Society: Washington, DC, 1994; Chapter 4, pp 56−65.
(5) Christe, K. O.; Curtis, E. C.; Dixon, D. A. *J. Am. Chem. Soc.* **1993**, *115*, 1520.
(6) Christe, K. O.; Dixon, D. A.; Sanders, J. C. P.; Schrobilgen, G. J.; Wilson, W. W. *J. Am. Chem. Soc.* **1993**, *115*, 9461.
(7) Christe, K. O.; Curtis, E. C.; Dixon, D. A. *J. Am. Chem. Soc.* **1993**, *115*, 9655.
(8) Drake, G. W.; Dixon, D. A.; Sheehy, J. A.; Boatz, J. A.; Christe, K. O. *J. Am. Chem. Soc.* **1998**, *120*, 8392.

10.1021/ic034457w CCC: $25.00
Published on Web 07/19/2003

members of this series have been established, except for the AO_2F_5 case. In this paper, the preparation and structure of the $IO_2F_5^{2-}$ anion, the first example of a main-group AO_2F_5 species, is reported.

Experimental Section

Materials and Apparatus. All volatile materials were handled in either Pyrex vacuum lines equipped with Kontes or J. Young glass−Teflon valves or a stainless steel, Teflon−FEP vacuum line.[15] Nonvolatile materials were handled in the dry nitrogen atmosphere of a glovebox.

The solvents, CH_3CN (Baker, HPLC Grade) and anhydrous HF (Harshaw), were dried according to literature methods[16] and distilled prior to their use. The syntheses of $[N(CH_3)_4][F]$[17] and IO_2F_3[18] have been described previously. Fluoroform, CHF_3 (Matheson, 99.995%), was used as received.

Preparation of $[N(CH_3)_4][IO_4]$. Tetramethylammonium metaperiodate, $[N(CH_3)_4][IO_4]$, was prepared either by the literature method[19] or by the following metathesis reaction. Approximately 30 mL of a 0.76 M aqueous solution of $[N(CH_3)_4][Cl]$ (Fluka Chemika, 98%) (22.80 mmol) was slowly added, with stirring, to 40 mL of aqueous $[Na][IO_4]$ (Matheson Coleman & Bell, 99.8%) (22.77 mmol). A white precipitate formed almost immediately, and the resulting mixture was stirred in an ice water bath for 30 min. The $[N(CH_3)_4][IO_4]$ precipitate was filtered off, washed with ice cold water, and dried for 15 h at 88 °C in a dynamic vacuum. $[N(CH_3)_4][IO_4]$ was obtained in a yield of 53.7% (3.2643 g). The infrared and Raman spectra of the product showed no detectable amounts of water.

Preparation of $[N(CH_3)_4][IO_2F_4]$. Tetramethylammonium tetrafluoroperiodate was prepared by analogy with a previously published[20] method. In the drybox, $[N(CH_3)_4][IO_4]$ (2.995 mmol) was loaded into a 20-cm long, $^1/_2$-in. o.d. Teflon−FEP tube that was closed by a Kel-F valve. On a metal line, anhydrous HF (3.4 mL) was distilled onto the $[N(CH_3)_4][IO_4]$. The mixture was allowed to warm to room temperature, giving a colorless solution, and agitated for 3 days on a mechanical shaker. The HF and H_2O were pumped off between 0 and 45 °C over a period of 14 h. Fresh anhydrous HF was distilled onto the sample, and the tube was agitated for an additional 2 days, followed by removal of the solvent in a dynamic vacuum to give $[N(CH_3)_4][IO_2F_4]$ in 96.8% yield in the form of a white, crystalline solid. The purity was verified by its low-temperature Raman spectrum, which showed the presence of a mixture of $[N(CH_3)_4][cis\text{-}IO_2F_4]$ and $[N(CH_3)_4][trans\text{-}IO_2F_4]$ ($cis\text{-}IO_2F_4^-$ (cm^{-1}): 207 (3), 235 (<0.5), 330 (35), 366 sh, 394 (19), $\nu_4(A_1)$; 560 (24), $\nu_3(A_1)$; 610 (74), $\nu_2(A_1)$; 847 (75), $\nu_1(A_1)$; 870 (13), 880 sh, $\nu_{12}(B_2)$. $trans\text{-}IO_2F_4^-$ (cm^{-1}): 251 (5), $\nu_6(B_{2g})$; 380 (41), $\nu_8(E_g)$; 560 (24), $\nu_5(B_{1g})$; 571 (65), $\nu_2(A_{1g})$; 813 (100), $\nu_1(A_{1g})$). Fluorine-19 NMR spectroscopy of $[N(CH_3)_4][IO_2F_4]$ in HF solution[20] indicated an approximate cis to trans isomer ratio of 70:30.

Alternatively, $[N(CH_3)_4][IO_2F_4]$ was prepared from IO_2F_3 and $[N(CH_3)_4][F]$. In a typical synthesis, IO_2F_3 (10.774 mmol) was condensed into a $^3/_8$-in. o.d. Teflon−FEP reaction tube equipped with a Kel-F valve, and 5 mL of anhydrous CH_3CN was condensed onto the solid at −196 °C. The IO_2F_3 completely dissolved, with agitation, upon warming to room temperature. The solution was transferred into a drybox and frozen in a −196 °C cold well, and $[N(CH_3)_4][F]$ (11.050 mmol) was added. The reactor was removed from the drybox and warmed to room temperature resulting in a colorless solution. Removal of the CH_3CN for several hours in a dynamic vacuum gave colorless, friable, microcrystalline $[N(CH_3)_4][IO_2F_4]$ (10.854 mmol). Its purity was established by Raman spectroscopy.

Caution! The condensation of IO_2F_3 onto frozen CH_3CN solutions can result in detonations when the mixtures are warmed to the melting point of the solvent**.**

Preparation of $[N(CH_3)_4]_2[IO_2F_5]$. Inside a drybox, $[N(CH_3)_4][IO_2F_4]$ (1.853 mmol) was added to one arm of a flamed-out, H-shaped glass reaction vessel equipped with a J. Young valve on each side and one separating the two arms. A stoichiometric amount of $[N(CH_3)_4][F]$ (1.882 mmol) was added to the other arm of the reaction vessel. Anhydrous CH_3CN was condensed at −196 °C into both arms (combined volume ca. 7 mL), and the reactor was warmed to −30 °C. The CH_3CN solution of $[N(CH_3)_4][F]$ was transferred into the arm of the reaction vessel containing the $[N(CH_3)_4][IO_2F_4]$ solution. The mixture was stirred at −30 °C for 2 h using a magnetic stir bar. The CH_3CN solvent was pumped off over a period of 16 h while slowly warming from −30 to 0 °C, yielding 0.7970 g of a fine, white powder consisting of $[N(CH_3)_4]_2[IO_2F_5]$, $[N(CH_3)_4][F]$, and $[N(CH_3)_4][cis\text{-}IO_2F_4]$.

Inside a drybox, part of the aforementioned $[N(CH_3)_4]_2[IO_2F_5]/[N(CH_3)_4][F]/[N(CH_3)_4][cis\text{-}IO_2F_4]$ mixture (0.3433 g) was loaded into one arm of the H-shaped reaction vessel. Approximately 2.5 mL of anhydrous CH_3CN was distilled onto the mixture in a static vacuum at −196 °C. The mixture was allowed to warm to −20 °C, was agitated, and then allowed to settle. After 2 h, the CH_3CN solution was decanted into the other arm of the reaction vessel, and the solvent was distilled back onto the solid residue. Washing of the solid was repeated 10 more times using 2.5 mL of CH_3CN solvent. The CH_3CN was then pumped off on a glass vacuum line over a period of 12 h while warming from −30 to 25 °C, yielding 0.1382 g of a fine, white powder that consisted, on the basis of its weight and vibrational spectra, of 75 wt % $[N(CH_3)_4]_2[IO_2F_5]$ and 25 wt % $[N(CH_3)_4][cis\text{-}IO_2F_4]$.

Alternatively, a previously described Teflon−FEP metathesis apparatus[21] was loaded in the drybox with $[N(CH_3)_4][F]$ (2.58 mmol) and $[N(CH_3)_4][IO_2F_4]$ (2.01 mmol). On a glass vacuum line, approximately 10 mL of CH_3CN was condensed onto the solid at −196 °C. After melting of the CH_3CN solvent at −31 °C, the reaction mixture was kept at −31 °C for 2 h and periodically stirred resulting in the formation of a large amount of white solid. The

(9) Christe, K. O.; Curtis, E. C.; Dixon, D. A.; Mercier, H. P. A.; Sanders, J. C. P.; Schrobilgen, G. J. *J. Am. Chem. Soc.* **1991**, *113*, 3351.
(10) Christe, K. O.; Wilson, W. W.; Drake, G. W.; Dixon, D. A.; Boatz, J. A.; Gnann, R. Z. *J. Am. Chem. Soc.* **1998**, *120*, 4711.
(11) Christe, K. O.; Dixon, D. A.; Mahjoub, A. R.; Mercier, H. P. A.; Sanders, J. C. P.; Seppelt, K.; Schrobilgen, G. J.; Wilson, W. W. *J. Am. Chem. Soc.* **1993**, *115*, 2696.
(12) Christe, K. O.; Dixon, D. A.; Sanders, J. C. P.; Schrobilgen, G. J.; Wilson, W. W. *Inorg. Chem.* **1993**, *32*, 4089.
(13) Christe, K. O.; Dixon, D. A.; Sanders, J. C. P.; Schrobilgen, G. J.; Tsai, S. S.; Wilson, W. W. *Inorg. Chem.* **1995**, *34*, 1868.
(14) Christe, K. O.; Wilson, W. W.; Dixon, D. A.; Boatz, J. A. *J. Am. Chem. Soc.* **1999**, *121*, 3382.
(15) Christe, K. O.; Wilson, R. D.; Schack, C. J. *Inorg. Synth.* **1986**, *24*, 3.
(16) (a) Winfield, J. M. *J. Fluorine Chem.* **1984**, *25*, 91. (b) Christe, K. O.; Wilson, W. W.; Schack, C. J. *J. Fluorine Chem.* **1978**, *11*, 71. (c) Emara, A. A. A.; Schrobilgen, G. J. *Inorg. Chem.* **1992**, *31*, 1323.
(17) Christe, K. O.; Wilson, W. W.; Wilson, R. D.; Bau, R.; Feng, J.-a. *J. Am. Chem. Soc.* **1990**, *112*, 7619.
(18) Engelbrecht, A.; Peterfy, P.; Schandara, E. *Z. Anorg. Allg. Chem.* **1971**, *384*, 202.
(19) Wagner, R. I.; Bau, R.; Gnann, R. Z.; Jones, P. F.; Christe, K. O. *Inorg. Chem.* **1997**, *36*, 2564.
(20) Christe, K. O.; Wilson, R. D.; Schack, C. J. *Inorg. Chem.* **1981**, *20*, 2104.
(21) Christe, K. O.; Schack, C. J.; Wilson, R. D. *Inorg. Chem.* **1977**, *16*, 849.

apparatus was inverted, and the reaction mixture was quickly pressure filtered, followed by removal of the CH_3CN in a dynamic vacuum at ambient temperature. Inside the drybox, the apparatus was disassembled and 0.550 g of a white solid from the filter cake (containing $[N(CH_3)_4]_2[IO_2F_5]$, $[N(CH_3)_4][cis\text{-}IO_2F_4]$, and trace amounts of $[N(CH_3)_4][trans\text{-}IO_2F_4]$) and 0.250 g of a white filtrate residue, containing $[N(CH_3)_4][F]$ and isomerically pure $[N(CH_3)_4][cis\text{-}IO_2F_4]$, were collected.

In another modification, clear solutions of $[N(CH_3)_4][F]$ (2.90 mmol) in 15 mL of CH_3CN and $[N(CH_3)_4][IO_2F_4]$ (2.04 mmol) in 7 mL of CH_3CN were combined inside a drybox in a 100-mL Teflon bottle. A copius white precipitate instantaneously formed that was pressure-filtered through a Teflon filter (Pall Corp.). The white filtercake was transferred into a 3/4-in. o.d. Teflon ampule equipped with a stainless steel valve and pumped to dryness for 2 h at ambient temperature. Vibrational spectroscopy of the filtercake showed the presence of $[N(CH_3)_4]_2[IO_2F_5]$, $[N(CH_3)_4][cis\text{-}IO_2F_4]$, and trace amounts of $[N(CH_3)_4][trans\text{-}IO_2F_4]$).

Vibrational Spectroscopy. The low-temperature Raman spectra were recorded either with a Jobin-Yvon model S-3000 spectrometer, using the 514.5-nm line of an Ar ion laser and an Olympus metallurgical microscope (model BHSM-L-2) for focusing the laser, a Cary model 83GT with 488-nm excitation from an Ar ion laser, or a Spex model 1403 with 647.1-nm excitation from a Kr ion laser. Spectra were recorded at low temperature using microcrystalline samples of $[N(CH_3)_4]_2[IO_2F_5]/[N(CH_3)_4][cis\text{-}IO_2F_4]$ sealed in Pyrex melting point capillaries. The infrared spectra were recorded on a Mattson Galaxy FTIR spectrometer using dry powders pressed between AgCl disks in a Wilks minipress.

Theoretical Calculations. Electronic structure calculations were done at the local density functional theory (LDFT)[22,23] and the Hartree−Fock (HF) level.[24] The LDFT calculations were done with a polarized valence double-ζ basis set (DZVP).[25] The HF calculations were done with a polarized valence double-ζ basis set augmented by diffuse functions[26] on O and F and a polarized valence double-ζ basis set on I with an effective core potential.[27] Geometries were optimized, and second derivatives were calculated at the optimized geometries. The initial LDFT calculations were done with DGauss[28] (using the A1 charge fitting basis set), and the final LDFT and HF calculations were done with Gaussian 98.[29] The second derivatives were analyzed by using the program BMATRIX developed by Komornicki.[30] Raman intensities were determined analytically at the HF level and numerically at the LDFT level. Because we did not use a large basis set with diffuse functions to obtain accurate polarizabilities, the Raman intensities provide only qualitative information.

Results and Discussion

Synthesis of $[N(CH_3)_4][IO_2F_4]$. The $N(CH_3)_4^+$ salt of the known $IO_2F_4^-$ anion was prepared by two synthetic routes. By analogy with the reported preparation of $[Cs][IO_2F_4]$,[20] a mixture of *cis*- and *trans*-$[N(CH_3)_4][IO_2F_4]$ in a 7:3 isomer ratio was obtained from $[N(CH_3)_4][IO_4]$ upon repeated treatments with a large excess of anhydrous HF (eq 1).

Alternatively, $[N(CH_3)_4][IO_2F_4]$ was synthesized by the reaction of IO_2F_3 with $[N(CH_3)_4][F]$ in CH_3CN solution (eq 2).

$$[N(CH_3)_4][IO_4] + 4HF \overset{HF}{\rightleftharpoons} [N(CH_3)_4][IO_2F_4] + 2H_2O \quad (1)$$

$$[N(CH_3)_4][F] + IO_2F_3 \xrightarrow{CH_3CN} [N(CH_3)_4][IO_2F_4] \quad (2)$$

Synthesis of $[N(CH_3)_4]_2[IO_2F_5]$. A mixture of *cis*- and *trans*-$[N(CH_3)_4][IO_2F_4]$ was allowed to react with 1 mol equiv of $[N(CH_3)_4][F]$ in CH_3CN either at −30 °C or at ambient temperature. The solvent was pumped off in a dynamic vacuum, yielding a white product consisting of $[N(CH_3)_4]_2[trans\text{-}IO_2F_5]$ and $[N(CH_3)_4][cis\text{-}IO_2F_4]$. The reaction was also carried out in CHF_3 solution at 0 °C, but these conditions are less convenient because of the high vapor pressure of the solvent and the presence of some unreacted $[N(CH_3)_4][trans\text{-}IO_2F_4]$ in the product. These results show that under the given reaction conditions only *trans*-$IO_2F_4^-$ reacts with F^-, yielding the *trans*-$IO_2F_5^{2-}$ anion according to eq 3.

$$[N(CH_3)_4][trans\text{-}IO_2F_4] + [N(CH_3)_4][F] \xrightarrow{CH_3CN \text{ or } CHF_3} [N(CH_3)_4]_2[trans\text{-}IO_2F_5] \quad (3)$$

(22) (a) Parr, R. G.; Yang, W. *Density-Functional Theory of Atoms and Molecules*; Oxford University Press: New York, 1989. (b) Labanowski, J. K., Andzelm, J. W., Eds. *Density Functional Methods in Chemistry*; Springer-Verlag: New York, 1991. (c) Ziegler, T. *Chem. Rev.* **1991**, *91*, 651. (d) Salahub, D. R. In *Ab Initio Methods in Quantum Chemistry-II*; Lawley, K. P., Ed.; J. Wiley & Sons: New York, 1987; p 447. (e) Jones, R. O.; Gunnarsson, O. *Rev. Mod. Phys.* **1989**, *61*, 689.

(23) Vosko, S. H.; Wilk, L.; Nusair, M. *Can. J. Phys.* **1980**, *58*, 1200. (Keyword = SVWN5 in Gaussian 98).

(24) (a) Hirst, D. M. *A Computational Approach to Chemistry*; Blackwell Scientific: Oxford, U.K., 1990. (b) Grant, G. H.; Richards, W. G. *Computational Chemistry*; Oxford University Press: Oxford, U.K., 1995. (c) Hehre, W. J.; Radom, L.; Schleyer, P. v. R.; Pople, J. A. *Ab Initio Molecular Orbital Theory*; John Wiley and Sons: New York, 1986.

(25) Godbout, N.; Salahub, D. R.; Andzelm, J.; Wimmer, E. *Can. J. Chem.* **1992**, *70*, 560. Basis sets were obtained from the Extensible Computational Chemistry Environment Basis Set Database developed in and distributed by the Molecular Science Computing Facility, William R. Wiley Environmental and Molecular Sciences Laboratory, Pacific Northwest National Laboratory. http://www.emsl.pnl.gov:2080/forms/basisform.html.

(26) Dunning, T. H., Jr.; Hay, P. J. In *Methods of Electronic Structure Theory*; Schaefer, H. F., III, Ed.; Plenum Press: New York, 1977; Chapter 1.

(27) (a) Hay, P. J.; Wadt, W. R. *J. Chem. Phys.* **1985**, *82*, 270. (b) Wadt, W. R.; Hay, P. J. *J. Chem. Phys.* **1985**, *82*, 284. (c) Hay, P. J.; Wadt, W. R. *J. Chem. Phys.* **1985**, *82*, 299.

(28) (a) Andzelm, J.; Wimmer, E.; Salahub, D. R. In *The Challenge of d and f Electrons: Theory and Computation*; Salahub, D. R., Zerner, M. C., Eds.; ACS Symposium Series, No. 394; American Chemical Society: Washington, DC, 1989; p 228. (b) Andzelm, J. In *Density Functional Theory in Chemistry*; Labanowski, J., Andzelm, J., Eds.; Springer-Verlag: New York, 1991; p 15. (c) Andzelm, J. W.; Wimmer, E. *J. Chem. Phys.* **1992**, *96*, 1280.

(29) Frisch, M. J.; Trucks, G. W.; Schlegel, H. B.; Scuseria, G. E.; Robb, M. A.; Cheeseman, J. R.; Zakrzewski, V. G.; Petersson, G. A.; Montgomery, J. A., Jr.; Stratmann, R. E.; Burant, J. C.; Dapprich, S.; Millam, J. M.; Daniels, A. D.; Kudin, K. N.; Strain, M. C.; Farkas, O.; Tomasi, J.; Barone, V.; Cossi, M.; Cammi, R.; Mennucci, B.; Pomelli, C.; Adamo, C.; Clifford, S.; Ochterski, J.; Petersson, G. A.; Ayala, P. Y.; Cui, Q.; Morokuma, K.; Malick, D. K.; Rabuck, A. D.; Raghavachari, K.; Foresman, J. B.; Cioslowski, J.; Ortiz, J. V.; Stefanov, B. B.; Liu, G.; Liashenko, A.; Piskorz, P.; Komaromi, I.; Gomperts, R.; Martin, R. L.; Fox, D. J.; Keith, T.; Al-Laham, M. A.; Peng, C. Y.; Nanayakkara, A.; Gonzalez, C.; Challacombe, M.; Gill, P. M. W.; Johnson, B.; Chen, W.; Wong, M. W.; Andres, J. L.; Head-Gordon, M.; Replogle, E. S.; Pople, J. A. *Gaussian 98*, A.7; Gaussian, Inc.: Pittsburgh, PA, 1998.

(30) Komornicki, A. *BMATRIX Version 2.0*; Polyatomics Research Institute: Palo Alto, CA, 1996.

Table 1. Observed and Calculated Vibrational Spectra of the *trans*-$O_2F_5^{2-}$ Anion and Their Assignment in Point Group D_{5h}

assgnt (activity)	approx mode description	obsd freq, cm^{-1} (rel intensity), for $[N(CH_3)_4]_2[IO_2F_5]$		scaled[f] calcd freq, cm^{-1} (IR, Ra intens)	
		Raman[a,b]	infrared[c,d]	LDFT/DZVP	HF/ECP/DZVP
A_1' (Ra)	ν_1, ν sym IO_2	789 [100]		781 (0) [37]	776 (0) [43]
	ν_2, ν sym IF_5	517 [57]		505 (0) [29]	505 (0) [27]
A_2'' (IR)	ν_3, ν as IO_2		847 s[e]	856 (150) [0]	861 (90) [0]
	ν_4, δ umbrella IF_5		330 m, sh[e]	338 (40) [0]	352 (86) [0]
E_1' (IR)	ν_5, ν as IF_5		490 vs	537 (591) [0]	503 (808) [0]
	ν_6, δ scissoring IO_2		390 s	389 (97) [0]	391 (291) [0]
	ν_7, δ as IF_5 in plane		not obsd	244 (0) [0]	251 (0) [0]
E_1'' (Ra)	ν_8, δ rock IO_2	368 [57]		340 (0) [13]	346 (0) [14]
E_2' (Ra)	ν_9, ν as IF_5	not obsd[g]		449 (0) [4]	442 (0) [0.6]
	ν_{10}, δ scissoring IF_5	395 [26][e]		393 (0) [7]	392 (0) [3.8]
E_2'' (i.a.)	ν_{11}, δ puckering IF_5			158 (0) [0]	176 (0) [0]

[a] Spectrum recorded on a microcrystalline solid in a Pyrex glass capillary at −113 °C using 514.5-nm excitation. [b] The $N(CH_3)_4^+$ cation modes were observed as follows (cm^{-1}): 380 (11), ν_8(E); 457 (13), ν_{19}(F_2); 752 (35), ν_3(A_1); 953 (22), ν_{18}(F_2); 1187 (3), ν_7(E); 1294 (3), ν_{17}(F_2); 1418 (5), ν_{16}(F_2); 1465 sh, ν_2(A_1); 1476 (31), ν_6(E); 2818 (4), 2828 (5), 2836 (5), 2899 sh, 2934 (16), 2970 (25), 2995 (15), 3038 (33), ν_{CH_3} and binary bands (see refs 17 and 33). The *cis*-$IO_2F_4^-$ anion modes were observed as follows (cm^{-1}): 209 (1), 331 (14), 356(3) sh, bending modes; 395 (26), ν_4(A_1); 567 (7), ν_3(A_1); 608 (26), ν_2(A_1); 854 (31), ν_1(A_1); 871 (5), ν_{12}(B_2) (see ref 20 and Table 3). Bands arising from residual CH_3CN were observed as follows (cm^{-1}): 916 (7), ν_4(A_1); 1378 (1), ν_3(A_1); 2247 (14), ν_2(A_1); 2944 (16) cm^{-1}, ν_1(A_1). [c] Spectrum recorded on a microcrystalline solid pressed between two AgCl disks. [d] The $N(CH_3)_4^+$ cation modes were observed as follows (cm^{-1}): 462 sh, ν_{19}(F_2); 922 w, $2\nu_{19}$; 955 vs, ν_{18}(F_2); 1257 mw, 1265 mw, 1288 mw, ν_{17}(F_2); 1420 m, ν_{16}(F_2); 1497 s, ν_{15}(F_2); 1774 w, br, 1943 w, vbr, 2340 w, 2362 w, 2499 w, 2589 w, 2998 m, 3046 s, 3411 vw, 3493 vw cm^{-1}, ν_{CH_3} and binary bands (see refs 17 and 35). The *cis*-$IO_2F_4^-$ anion modes were observed as follows (cm^{-1}): 354 vs; 367 vs, ν_5(A_1); 564 sh, ν_3(A_1); 620 vs, br, ν_2(A_1) and ν_9(B_1); 847 vs, ν_1(A_1); 871 vs, ν_{12}(B_2) (see ref 20 and Table 3). [e] These $IO_2F_5^{2-}$ anion bands overlap with bands of the *cis*-$IO_2F_4^-$ anion. [f] The following empirical scaling factors were used to obtain the best fit with the observed frequencies: LDFT, I−O stretching modes, 1.0622; remaining modes, 1.1081; HF, I−O stretching modes, 1.0436; remaining modes, 0.9388. [g] Obscured by the 457-cm^{-1} Raman band of $N(CH_3)_4^+$.

The observation that only the *trans*-$IO_2F_4^-$ ion reacts with the F^- ion can be rationalized by kinetic effects. Because the oxygen double bond domains are larger and more repulsive than those of the fluorine single bonds,[2,31] the F^- ion approaches the $IO_2F_4^-$ ion in the direction of the least repulsion, i.e., through a triangular F_3 face in the case of *cis*-$IO_2F_4^-$ and through an F_2O face in the case of *trans*-$IO_2F_4^-$. In the latter case, the additional fluorine ligand can easily slip into the existing equatorial fluorine belt, resulting directly in the energetically favored *trans*-$IO_2F_5^-$ structure of D_{5h} symmetry. In the case of *cis*-$IO_2F_4^-$, however, the analogous approach results in an intermediate structure that cannot easily rearrange to D_{5h} symmetry without the kinetically unfavorable, complete breakage and re-formation of an I−F bond. This argument also accounts for the lack of easy cis/trans isomerization in pseudooctahedral species, such as $IO_2F_4^-$, and the ease of this isomerization in pseudotrigonal-bipyramidal species through a Berry pseudorotation mechanism.[32]

Although most of the unreacted $[N(CH_3)_4][$*cis*-$IO_2F_4]$ salt can be extracted from the product mixture using CH_3CN, not all of the $[N(CH_3)_4][$*cis*-$IO_2F_4]$ was removed even after numerous washings. Removal of the solvent from the washings afforded isomerically pure $[N(CH_3)_4][$*cis*-$IO_2F_4]$, containing some $[N(CH_3)_4][F]$, as shown by infrared spectroscopy. Although isomerically pure *trans*-$IO_2F_4^-$ had previously been prepared,[33] this procedure represents the first isolation of isomerically pure *cis*-$IO_2F_4^-$.

Attempts to grow single crystals of $[N(CH_3)_4][$*cis*-$IO_2F_4]$ from the CH_3CN extract of the crude $[N(CH_3)_4]_2[IO_2F_5]$/$[N(CH_3)_4][$*cis*-$IO_2F_4]$/$[N(CH_3)_4][F]$ reaction product mixture yielded crystals of $[N(CH_3)_4]_2[IO_2F_2][HF_2]$ instead.[34] The reducing agent required for the reduction of $I^{+VII}O_2F_4^-$ to $I^{+V}O_2F_2^-$ is most likely CH_3CN. Tetramethylammonium fluoride may play a crucial role in this reduction because it is known to readily abstract a proton from CH_3CN yielding the CH_2CN^- anion.[17]

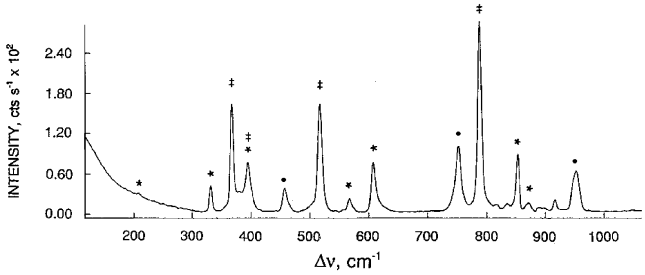

Figure 1. Raman spectrum of $[N(CH_3)_4]_2[IO_2F_5]$ containing about 25 wt % of $[N(CH_3)_4][$*cis*-$IO_2F_4]$, recorded at −113 °C using 514.5-nm excitation. The *trans*-$IO_2F_5^{2-}$, *cis*-$IO_2F_4^-$, and $N(CH_3)_4$ bands are indicated by ‡, *, and ●, respectively.

Vibrational Spectra and Structure of the *trans*-$IO_2F_5^{2-}$ Anion. The Raman spectrum of $[N(CH_3)_4]_2[IO_2F_5]$ containing about 25 wt % of $[N(CH_3)_4][$*cis*-$IO_2F_4]$ is shown in Figure 1. The observed vibrational frequencies for $IO_2F_5^{2-}$ and their assignments based on the theoretical calculations are summarized in Table 1. After subtraction of the bands belonging to the $N(CH_3)_4^+$ cation,[35] the *cis*-$IO_2F_4^-$ anion, and trace amounts of CH_3CN, four new Raman bands at 789, 517, 395, and 368 cm^{-1} and four new infrared bands at 847, 490, 390, and 330 cm^{-1} remain that can be assigned to the novel pentagonal-bipyramidal $IO_2F_5^{2-}$ anion of D_{5h} symmetry with the oxygen atoms in the two axial positions (see Figure 2).

(31) Gillespie, R. J.; Robinson, E. A. *Angew. Chem., Int. Ed. Engl.* **1996**, *35*, 495.
(32) Berry, R. S. *J. Chem. Phys.* **1960**, *32*, 933.
(33) Gillespie, R. J.; Krasznai, J. P. *Inorg. Chem.* **1977**, *16*, 1384.
(34) Gerken, M.; Schrobilgen, G. J. *J. Fluorine Chem.*, to be submitted for publication.
(35) Berg, R. W. *Spectrochim. Acta, Part A* **1978**, *34A*, 655.

Table 2. Comparison of the Vibrational Frequencies of the Pentagonal Planar IF_5 Moiety in *trans*-$IO_2F_5^{2-}$ with Those of IF_7, IOF_6^-, IOF_5^{2-}, and IF_5^{2-} in Point Group C_{5v}

		compd (oxdn state)				
		replacemt. of F by O^-			replacemt of O by free valence el pair	
assignt	approx mode description	IF_7 (+VII) [5]	IOF_6^- (+VII) [11]	$IO_2F_5^{2-}$ (+VII)	IOF_5^{2-} (+V) [14]	IF_5^{2-} (+III) [10]
A_1	ν sym IF_5	635	584	517	485	474
	δ umbrella IF_5	365	359	330	289	[307][a]
E_1	ν asym IF_5	670	585	490	334	335
	δ as IF_5 in plane	425	405	[250]	254	245
E_2	ν asym IF_5	596	530	[450]	367/355	339/325
	δ scissoring IF_5	510	457	395	409	396
	δ puckering IF_5	[68]	[59]	[160]	[115]	[100]

[a] Values in brackets are calculated frequencies.

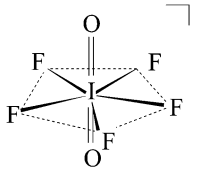

Figure 2. D_{5h} geometry of the *trans*-$IO_2F_5^{2-}$ anion.

A total of 18 vibrational modes are expected for the $IO_2F_5^{2-}$ anion of D_{5h} symmetry which span the irreducible representations $\Gamma = 2A_1' + 3E_1' + 2E_2' + 2A_2'' + E_1'' + E_2''$. Of the resulting 11 fundamental vibrations, 5 are Raman active ($2A_1'$, $2E_2'$, and E_1''), 5 are infrared active ($2A_2''$ and $3E_1'$), and the E_2'' mode is inactive. Of the expected five Raman and five infrared active vibrations, four were observed in each spectrum. The Raman band at 789 and the infrared band at 847 cm^{-1} represent the symmetric ($\nu_1(A_1')$) and antisymmetric ($\nu_3(A_2'')$) stretching modes of the axial IO_2 unit, respectively. Their large frequency separation and mutual exclusion establish, beyond doubt, the linearity (trans arrangement) of the O−I−O group. For the cis configuration and the monocapped octahedral and monocapped trigonal prismatic geometries, the symmetric and the antisymmetric IO_2 stretching modes would be both Raman and infrared active. This conclusion is further supported by a comparison with the spectra of *trans*-$IO_2F_4^-$ in its $N(CH_3)_4^+$ salt, where the mutually exclusive IO_2 stretching modes were observed at 813 and 880 cm^{-1}.[20] The observed decreases in frequency from $IO_2F_4^-$ to $IO_2F_5^{2-}$ are consistent with the greater I−O bond polarity in the $IO_2F_5^{2-}$ anion resulting from the increased negative formal charge of the dianion (see below).

Similarly, the Raman band at 517 cm^{-1}, which corresponds to the symmetric stretching mode, $\nu_2(A_1')$, of the five equatorial I−F bonds, is considerably lower in frequency than the corresponding band found at 571 cm^{-1} for the four I−F bonds in *trans*-$IO_2F_4^-$. The second Raman active IF_5 stretching mode, $\nu_9(E_2')$, was not observed because of its low intensity and interference with the 457-cm^{-1} band of $N(CH_3)_4^+$. The infrared active antisymmetric IF_5 stretching mode, $\nu_5(E_1')$, was observed as a very strong infrared band at 490 cm^{-1}, in accord with the predicted frequency and intensity values. The Raman band at 368 cm^{-1} is assigned to the IO_2 rocking mode, $\nu_8(E_1'')$, of $IO_2F_5^{2-}$, in accord with its predicted frequency and high Raman intensity.[11,12] The only remaining Raman band occurs at 395 cm^{-1}, in excellent agreement with the frequency predictions for the IF_5 scissoring mode, $\nu_{10}(E_2')$. Of the three expected infrared active deformation modes, the IO_2 scissoring mode, $\nu_6(E_1')$, and the IF_5 umbrella deformation mode, $\nu_4(A'')$, were observed at the expected frequencies. The remaining antisymmetric IF_5 in-plane deformation mode, $\nu_7(E_1')$, was not observed because of its low frequency and predicted near-zero infrared intensity. The observed vibrational spectra are in excellent agreement with the qualitative predictions and calculated frequencies for *trans*-$IO_2F_5^{2-}$ of D_{5h} symmetry and confirm the existence and symmetry of this novel anion beyond doubt.

The pentagonal-bipyramidal D_{5h} geometry of $IO_2F_5^{2-}$ is in accord with the VSEPR models[2] and with the structures previously established for IF_5^{2-} and IOF_5^{2-}.[10,14] All three anions possess a pentagonal IF_5 plane with the two axial positions occupied by free valence electron pairs or oxygen atoms. This is in accord with the doubly bonded oxygen and the free valence electron pair domains being more repulsive than those of the fluorine ligands[2] and, therefore, occupying the less crowded axial positions. In this manner, they achieve maximum avoidance.

It is interesting to examine the frequency trends for the pentagonal planar IF_5 group within the IF_7, IOF_6^-, $IO_2F_5^{2-}$, IOF_5^{2-}, and IF_5^{2-} series. In the isoelectronic IF_7, IOF_6^-, and $IO_2F_5^{2-}$ sequence, the oxidation state of iodine remains the same (+VII), whereas the axial fluorine ligands are stepwise replaced by formally negatively charged O ligands thereby increasing the overall negative charges. In the $IO_2F_5^{2-}$, IOF_5^{2-}, and IF_5^{2-} sequence, the axial oxygen ligands are stepwise replaced by free valence electron pairs, resulting in a stepwise reduction of the iodine oxidation state from +VII to +III.

As shown in Table 2, the IF_5 stretching modes are most strongly influenced by the ionic charges and the resulting polarity of the I−F bonds and to a lesser extent by the replacement of oxygen by a free valence electron pair. Similarly, the IF_5 in-plane deformation frequencies decrease with an increase in the ionic charge but change only little upon replacement of an oxygen ligand by a free valence electron pair, especially upon replacement of the second oxygen atom by a second free valence electron pair. The out-of-plane deformation modes change much less. Apparently, the lengthening and weakening of the I−F bonds by their increasing polarity is counteracted by the increased repulsion resulting from the replacement of an axial fluorine ligand by either a more repulsive oxygen ligand or a free valence electron pair.

Table 3. Observed and Calculated Vibrational Spectra of the *cis*-$IO_2F_4^-$ Anion and Their Assignment in Point Group C_{2v}

		obsd freq, cm^{-1} (rel intens)					scaled[b] calcd freq, cm^{-1} (IR, Ra intens)	
		$N(CH_3)_4IO_2F_4$		$CsIO_2F_4$[a]				
assgnt (activity)	approx mode description	Raman (solid)	infrared (solid)	Raman (solid)	infrared (solid)	Raman (CH_3CN soln)	LDFT/DZVP	HF/ECP/DZVP
A_1 (IR, Ra)	ν_1, ν sym IO_2	847 [100]	844 s	856 [100]	855 vs	851 [90] p	863 (73) [22]	868 (87) [29.9]
	ν_2, sym comb of ν sym IF_{2eq} and ν sym IF_{2ax}	608 [85]	605 s	605 [98]	600 vs, br	609 [100] p	593 (106) [30]	612 (134) [26.1]
	ν_3, asym comb of ν sym IF_{2eq} and ν sym IF_{2ax}	560 [24]	565 sh	552 sh	560 vw	540 [100] p	542 (0) [11]	556 (6) [6.3]
	ν_4, δ sciss IO_2	394 [15]	393 vw	394 [34]	395 sh	c	377 (0) [4.6]	383 (20) [2.2]
	ν_5, sym comb of δ sciss IF_{2eq} and δ sciss IF_{2ax}	370 [20]	370 s	369 [30]	364 s	355 sh[c]	366 (41) [3.2]	364 (92) [4.4]
	ν_6, asym comb of δ sciss IF_{2eq} and δ sym IF_{2ax}	207 [3]		210 [0.5]			208 (0) [0.13]	227 (0.1) [0.1]
A_2 (-, Ra)	ν_7, torsion IO_2	330 [38]	329 vw	332 [65]	328 w	335 sh	294 (0) [3.3]	320 (0) [3.4]
	ν_8, torsion IF_{2eq}						172 (0) [0.1]	196 (0) [0.1]
B_1 (IR, Ra)	ν_9, ν as IF_{2ax}	610[d]	613 vs		600 vs, br		614 (205) [1.1]	615 (280) [1.3]
	ν_{10}, δ rock IO_2		353 s		350 s		341 (35) [1.3]	360 (94) [0.9]
	ν_{11}, δ rock IF_{2eq}	330 [38]	329 vw	332 [65]	328 w	335 sh	287 (0) [4.4]	321 (1) [2.5]
B_2 (IR, Ra)	ν_{12}, ν as IO_2	868 [7]	868 vs	875 d	875 vs	870 sh	884 (114) [6.7]	885 (122) [9.0]
	ν_{13}, ν as IF_{2eq}		555 m		550 mw		551 (32) [3.3]	533 (41) [1.6]
	ν_{14}, sym comb of δ sciss OIF_e and FIF_{ax}	370 [20]	370 s	365 sh	364 s	355 sh[c]	365 (48) [0.70]	371 (115) [0.6]
	ν_{15}, asym comb of δ sciss OIF_e and FIF_{ax}						209 (0) [0.002]	227 (0) [0]

[a] Data from ref 20. [b] Empirical scaling factors were used to maximize the fit between observed and calculated frequencies; factors of 1.06 and 1.122 were used for the LDFT values of the stretching and deformation modes, respectively, and factors of 1.0, 0.9238, and 0.8615 were used for the HH/ECP values of the IO stretching, the IF stretching, and the deformations modes, respectively. [c] Interference from a strong solvent band. [d] Intensities were omitted because of coincidences with other modes which contribute more strongly to the intensity.

Although no main group D_{5h} AO_2X_5 species had previously been reported, the crystal structure[36] and vibrational spectra[37,38] of pentagonal-bipyramidal $UO_2F_5^{3-}$ are known. A comparison of its vibrational frequencies and assignments with those of *trans*-$IO_2F_5^{2-}$ shows reasonable agreement.

Vibrational Spectra of $[N(CH_3)_4][cis\text{-}IO_2F_4]$. The availability of vibrational spectra for isomerically pure $[N(CH_3)_4][cis\text{-}IO_2F_4]$ and calculated frequencies and intensities, combined with the previous data for the isomerically impure cesium salt,[20] permitted the conclusive assignments of the vibrational frequencies for this anion (see Table 3). With the exception of ν_6 and ν_{15}, which have vanishingly small infrared and Raman intensities on the basis of theoretical predictions, all fundamental vibrations can be assigned to the experimentally observed frequencies, assuming double coincidences for ν_5/ν_{14} and ν_7/ν_{11}, respectively. This assumption is supported by the theoretical calculations which predict that their frequencies are almost identical. The observed spectra are in accord with the theoretical predictions and those of the closely related *cis*-OsO_2F_4 molecule,[39] which exhibits a very similar spectrum. The following geometry was calculated for *cis*-$IO_2F_4^-$ at the HF/ECP/DZVP level of theory: I−O 1.731 Å; I−F_{ax} = 1.843 Å; I−F_{eq} = 1.856 Å; O−I−O =104.4°; O−I−F_{ax} = 95.3°; O−I−F_{eq} = 89.3°; F_{eq}–I−F_{eq} = 77.0°. The energy of the cis isomer is 3.3, 2.3, and 1.8 kcal/mol higher than that of the trans isomer at the HF/ECP, NLDFT, and LDFT levels of theory, respectively. The calculated I−O and I−F bond lengths in the cis isomer are very similar to those of the trans isomer (I−O = 1.731 Å and I−F = 1.855 Å) at the same level of theory.

Theoretical Calculations

Normal Coordinate Analysis of *trans*-$IO_2F_5^{2-}$. Because doubly charged anions, such as $IO_2F_5^{2-}$, exhibit only very little solubility in common solvents and, in solution, revert to the singly charged anions and free fluoride, it was not possible to grow single crystals for X-ray diffraction or to record solution NMR spectra. Therefore, theoretical calculations of the vibrational frequencies and intensities and their fit with the observed spectra were used to determine the structure of $IO_2F_5^{2-}$ and to evaluate the structural trends resulting from changes in the formal ionic charge, the oxidation state and coordination number (CN) of iodine, and the replacement of an oxygen ligand by either a free valence electron pair or a fluorine ligand. Because our previous work had shown[5−14] that for closely related iodine and xenon compounds HF/ECP/DZVP and LDFT/DZVP calculations, after appropriate scaling, approximate the experimental values quite well, the same approach was chosen for this study.

As shown in Table 1, there is good agreement between the observed and calculated frequencies and intensities for $IO_2F_5^{2-}$, thus confirming its D_{5h} geometry (see Figure 2). On the basis of a general comparison of calculated and experimental geometries for the closely related six-coordinated series $IO_2F_4^-$, IOF_4^-, IF_4^-, IOF_5, IF_5, and IF_6^+ and the seven-coordinated series $IO_2F_5^{2-}$, IOF_5^{2-}, IF_5^{2-}, IOF_6^-, IF_6^-, and IF_7 (see Figures 3 and 4, respectively), the following bond lengths are predicted for *trans*-$IO_2F_5^{2-}$: r_{I-F} = 1.97 Å and r_{I-O} = 1.78 Å (see Table 4).

In view of the importance of the vibrational spectra for the identification of the novel *trans*-$IO_2F_5^{2-}$ anion, a normal coordinate analysis was carried out using the scaled LDFT/DZVP frequencies from Table 1. The results are summarized in Table 5 and confirm the assignments and approximate mode descriptions given in Table 1. As can be seen from the potential energy distribution (PED) in Table 5, all modes are highly characteristic, except for ν_6 and ν_7 which are

(36) Zachariasen, W. H. *Acta Crystallogr.* **1954**, *7*, 783.
(37) (a) Dao, N. Q. *Bull. Soc. Chim. Fr.* **1968**, 3976. (b) Dao, N. Q.; Knidiri, M. *Spectrochim. Acta* **1976**, *32A*, 1113. (c) Knidiri, M.; Benarafa, L. *C. R. Hebd. Seances Acad. Sci., Ser. C* **1978**, *287*, 55−58.
(38) (a) Flint, C. D.; Tanner, P. A. *Mol. Phys.* **1981**, *43*, 933. (b) Tanner, P. A. *J. Chem. Soc., Faraday Trans. 2* **1984**, *80*, 365.
(39) Christe, K. O.; Dixon, D. A.; Mack, H. G.; Oberhammer, H.; Pagelot, A.; Sanders, J. C. P.; Schrobilgen, G. J. *J. Am. Chem. Soc.* **1993**, *115*, 11279.

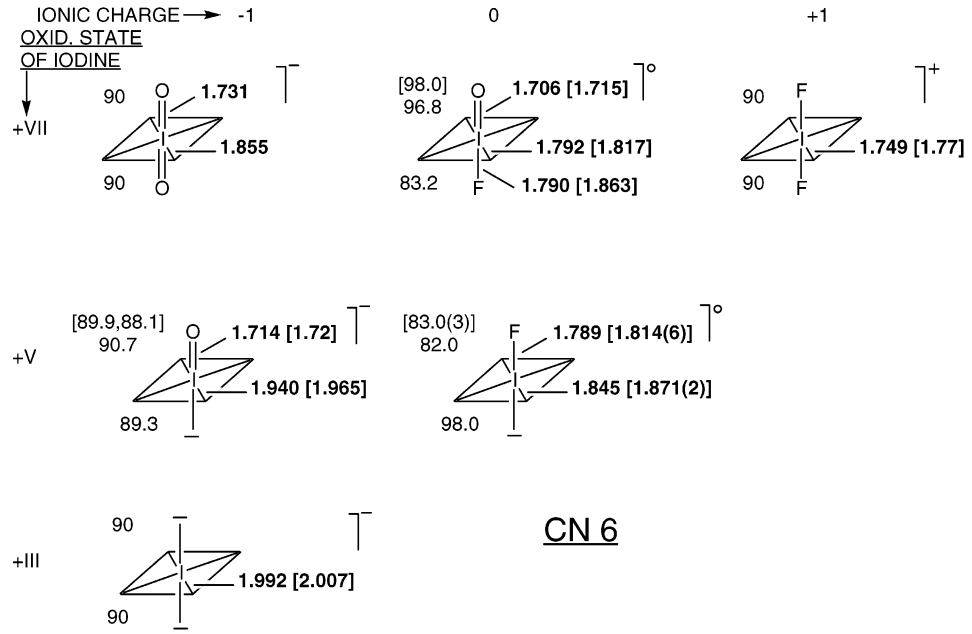

Figure 3. Geometries of the hexacoordinated $IO_2F_4^-$, IOF_4^-, IF_4^-,IOF_5, IF_5, and IF_6^+ ions and molecules, calculated in this study at the HF/ECP/DZVP level of theory. The calculated bond lengths (Å) and bond angles (deg) are given in bold and regular fonts, respectively, and the experimentally observed values (IF_6^+: unpublished data from our laboratories. IOF_5: ref 45. IOF_4^-: Ryan, R. R.; Asprey, L. B. *Acta Crystallogr, Sect. B* **1972**, *B28*, 979. IF_5: Balikci, B.; Brier, P. N. *J. Mol. Spectrosc.* **1981**, *89*, 254. IF_4^-: Zhang, X.; Seppelt, K. *Z. Anorg. Allg. Chem.* **1997**, *623*, 491) are shown in brackets.

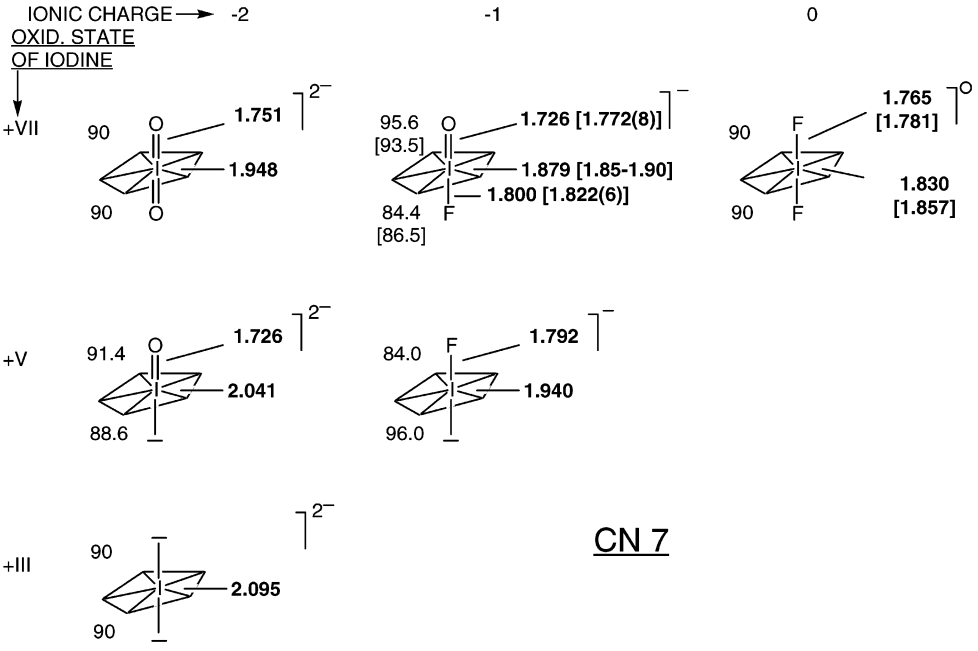

Figure 4. Geometries of the heptacoordinated $IO_2F_5^{2-}$, IOF_5^{2-}, IF_5^{2-}, IOF_6^-, IF_6^-, and IF_7 ions and molecules, calculated in this study at the HF/ECP/DZVP level of theory. The calculated bond lengths (Å) and bond angles (deg) are given in bold and regular fonts, respectively, and the experimentally observed values (IOF_6^-: ref 11. IF_7: Adams, W. J.; Thompson, B. H.; Bartell, L. S. *J. Chem. Phys*. **1970**, *53*, 4040) are shown in brackets. Despite IF_6^- having a monocapped octahedral structure in its $N(CH_3)_4^+$ salt,[40] a pseudopentagonal-bipyramidal structure was used for our study to allow a better comparison with the other members of this series.

symmetric and antisymmetric combinations, respectively, of the IO_2 scissoring and the IF_5 antisymmetric in plane deformation motions. The I−O and I−F stretching force constants have values of about 5.64 and 2.42 mdyn/Å, respectively, and correlate well with the predicted bond distances.

Analysis of *cis*-$IO_2F_5^{2-}$. The stability of cis isomers of $IO_2F_5^{2-}$ was also explored computationally at the LDFT/DZVP level of theory. Only one stable cis isomer was found which is shown in Figure 5. It possesses one axial and one

Table 4. Calculated Unscaled and Predicted Geometries for $IO_2F_5^{2-}$

	HF/ECP/DZVP	LDFT/DZVP	predicted
R(I−F), Å	1.948	2.057	1.97
R(I−O), Å	1.751	1.824	1.78
∠F−I−O, deg	90	90	90
∠F−I−F, deg	72	72	72

Table 5. Symmetry Force Constants[a] and Potential Energy Distribution[b] of D_{5h} $IO_2F_5^{2-}$ Calculated from the Scaled LDFT/DZVP Second Derivatives

	freq, cm^{-1}			
	obsd	calcd	sym force consts	PED, %
A_1'	789	781	$F_{11} = 5.74$	100 (1)
			$F_{12} = 0.128$	
	517	505	$F_{22} = 2.86$	100 (2)
A_2''	847	856	$F_{33} = 5.54$	95 (3)
			$F_{34} = 0.225$	
	330	338	$F_{44} = 1.70$	100 (4)
E_1'	490	537	$F_{55} = 2.45$	90 (5) + 7 (6) + 2 (8)
			$F_{56} = -0.521$	
			$F_{57} = 0.195$	
	390	389	$F_{66} = 2.45$	78 (6) + 21 (7)
			$F_{67} = -0.450$	
		244	$F_{77} = 1.18$	58 (6) + 41 (7)
E_1''	368	340	$F_{88} = 0.947$	100 (8)
E_2'		449	$F_{99} = 2.18$	88 (9) + 12 (10)
			$F_{9,10} = 0.194$	
	395	393	$F_{10,10} = 2.11$	84 (10) + 15 (9)
E_2''		158	$F_{11,11} = 0.598$	100 (11)

[a] Stretching constants in mdyn/Å, deformation constants in mdynÅ/rad^2, and stretch−bend interactions constants in mdyn/rad. The force constants were scaled with the square of the scaling factors used for the corresponding frequencies. [b] Symmetry coordinates: $S_1 = \nu$ sym IO_2; $S_2 = \nu$ sym IF_5; $S_3 = \nu$ asym IO_2; $S_4 = \delta$ umbrella IF_5; $S_5 = \nu$ asym IF_5; $S_6 = \delta$ scissoring IO_2; $S_7 = \delta$ asym IF_5 in plane; $S_8 = \delta$ rock IO_2; $S_9 = \nu$ asym IF_5; $S_{10} = \delta$ scissoring IF_5; $S_{11} = \delta$ puckering IF_5.

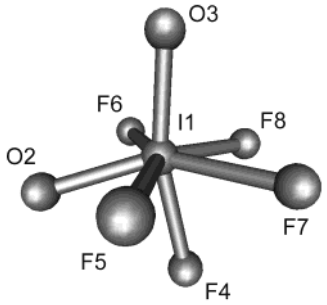

Figure 5. Minimum energy structure of the *cis*-$IO_2F_5^{2-}$ anion calculated at the LDFT/DZVP level.

equatorial oxygen atom and is 19.6 kcal/mol higher in energy than the trans isomer. The equatorial oxygen ligand requires more space than the fluorine ligands and is displaced from the equatorial plane by about 20°. This displacement causes a tilt of the adjacent axial fluorine ligand by about 14°. The remaining $O_{ax}IF_4$ fragment of the ion is part of an almost perfect pentagonal bipyramid. The geometry and unscaled vibrational frequencies of the cis isomer of $IO_2F_5^{2-}$ are summarized in Table 6. The poor correspondence between calculated and observed frequencies and intensities rules out the possibility of assigning the observed spectra to the cis isomer.

General Trends. Figures 3 and 4 also allow us to study the influence of the coordination number and oxidation state of iodine and of the ionic charge on the structures of these species. Because the HF/ECP/DZVP bond lengths approximate the experimental values better than the LDFT/DZVP results, the former values were used. Despite IF_6^- having a monocapped octahedral structure in its $N(CH_3)_4^+$ salt,[40] a pseudo-pentagonal-bipyramidal structure was used for our study to allow a better comparison with the other

Table 6. Geometry and Unscaled Vibrational Frequencies of the Cis Isomer of $IO_2F_5^{2-}$ Calculated at the LDFT/DZVP Level of Theory in Point Group C_s

		geometry			
	freq, cm^{-1} (IR intens)	bond lengths, Å		bond angles, deg	
A′	780.6 (123)	I−O2	1.846	O2−I−O3	110.0
	734.5 (86)	I−O3	1.830	O2−I−F4	85.2
	477.0 (135)	I−F4	2.038	O2−I−F5	78.0
	439.4 (30)	I−F5	2.100	O3−I−F5	89.6
	422.3 (0.25)	I−F7	2.066	O3−I−F7	91.2
	372.9 (5.7)			F4−I−F5	93.7
	337.4 (66)			F4−I−F7	76.3
	323.3 (37)			F5−I−F7	68.4
	303.9 (4.4)			F7−I−F8	69.1
	224.2 (0.03)				
	91.3 (0)				
A″	455.5 (258)				
	423.0 (2.2)				
	367.9 (72)				
	350.3 (1.3)				
	282.3 (0.08)				
	205.7 (0.03)				
	28.5 (0.08)				

members of this series. This is not unreasonable because the three possible structures, a monocapped octahedron, a pentagonal bipyramid, and a monocapped trigonal prism, are very close in energy.[1,41] An analysis of these figures reveals the following effects:

(i) The hexa- and heptacoordinated compounds exhibit similar general trends, except for the bonds in the heptacoordinated compounds being longer than those in the hexacoordinated ones. Whereas this difference is more pronounced for the equatorial iodine−fluorine bonds (∼8−10 pm), it is much smaller (∼1−2 pm) for the other bonds.

This observation might be explained by either the ability of the equatorial fluorine ligands to participate in the formation of semi-ionic, multicenter bonds[9,42−44] or, in the case of the heptacoordinated species, in terms of increased repulsion[2] of the ligands in the more crowded equatorial plane. Although any attempts to describe bonding situations are always flawed by our limited understanding of nature, we prefer the multicenter bonding arguments over the ligand repulsion model, particularly for cases such as pseudo-hexacoordinated IF_4^- which does not experience increased equatorial ligand crowding. It appears that the orthogonality of the sp^n and p orbitals is the main cause for the observed geometries in main group element compounds and that the observed bond elongations are the result of the equatorial p orbitals forming more than one bond, thereby contributing less electron density to the resulting bonds. In our opinion, repulsion effects are not the cause for this situation but an attempt to explain the experimentally observed facts by a simple and plausible model. If only repulsion and not the orthogonality of the orbitals were the main cause for the observed geometries, the molecules could readily avoid the

(40) Mahjoub, A.-R.; Seppelt, K. *Angew. Chem., Int. Ed. Engl.* **1991**, *30*, 323.
(41) Mahjoub, A.-R.; Drews, T.; Seppelt, K. *Angew. Chem., Int. Ed. Engl.* **1992**, *31*, 1036.
(42) Pimentel, G. C. *J. Chem. Phys.* **1951**, *19*, 446.
(43) Hach, R. J.; Rundle, R. E. *J. Am. Chem. Soc.* **1951**, *73*, 4321.
(44) Rundle, R. E. *J. Am. Chem. Soc.* **1963**, *85*, 112.

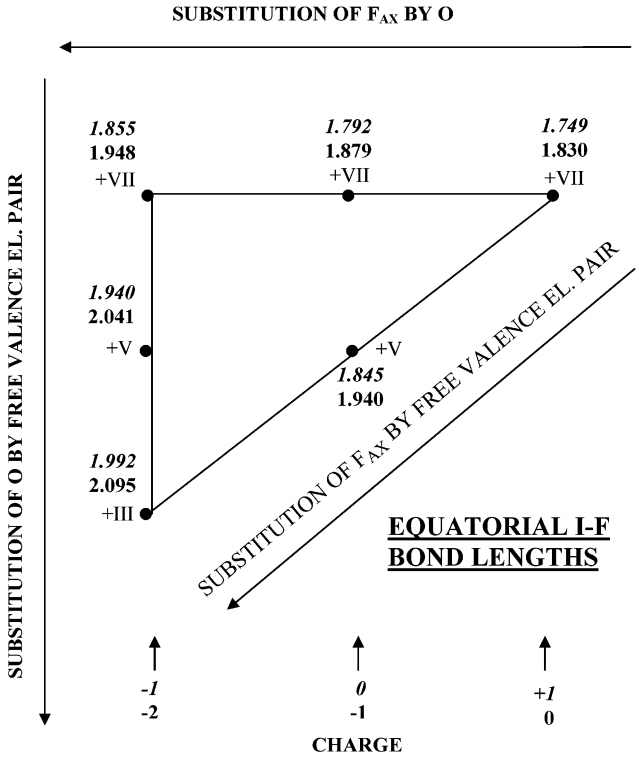

Figure 6. Changes of the equatorial I−F bond lengths (Å) with increasing ion charge and decreasing oxidation state of the central iodine atom. The arrangement of the individual compounds is identical with those in Figures 3 and 4, and the italic and nonitalic numerals represent the hexa- and heptacoordinated species, respectively.

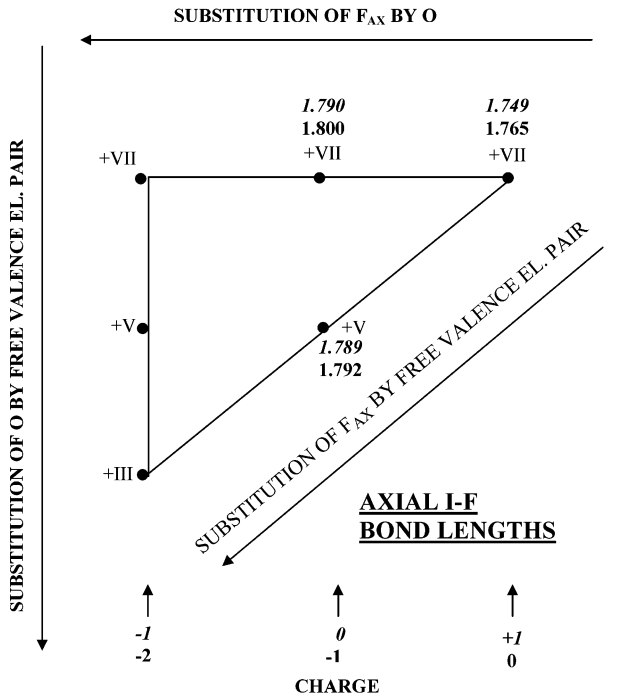

Figure 7. Changes of the axial I−F bond lengths (Å) with increasing ion charge and decreasing oxidation state of the central iodine atom. Italic and nonitalic numerals represent the hexa- and heptacoordinated species, respectively.

increased equatorial repulsion by puckering while maintaining identical bond lengths.

(ii) The equatorial I−F bond lengths are most strongly influenced by the ionic charges of the ions and the oxidation state of the central iodine atom (see Figure 6). This is not surprising in view of statement i, because both an increased negative charge and a reduced effective electronegativity of the central atom increase the ionicity of the equatorial I−F bonds.

(iii) The axial I−F bonds are more covalent and, therefore, similar in the hexa- and heptacoordinated species. They also gain substantial ionicity from an increase in the ion charge (see Figure 7).

(iv) The axial I−O bonds are also similar in the hexa- and heptacoordinated species but are much less influenced by changes in either the ion charge or the oxidation state of the central atom (see Figure 8).

(v) As one might expect, the replacement of axial fluorine ligands by less electron withdrawing oxygen ligands and the replacement of oxygen ligands by electron-feeding free valence electron pairs both decrease the effective electronegativity of the central atom and, thereby, increase the ionicity of the remaining I−F bonds. However, because these changes always go hand-in-hand with changes in the ion charge and the oxidation state of the central atom, they cannot be assessed independently in a more quantitative manner. The combination of these effects causes IF_6^+, with a positive ion charge, an iodine oxidation state of VII, a CN of 6, and no oxygen ligands or free iodine valence electron pairs, to

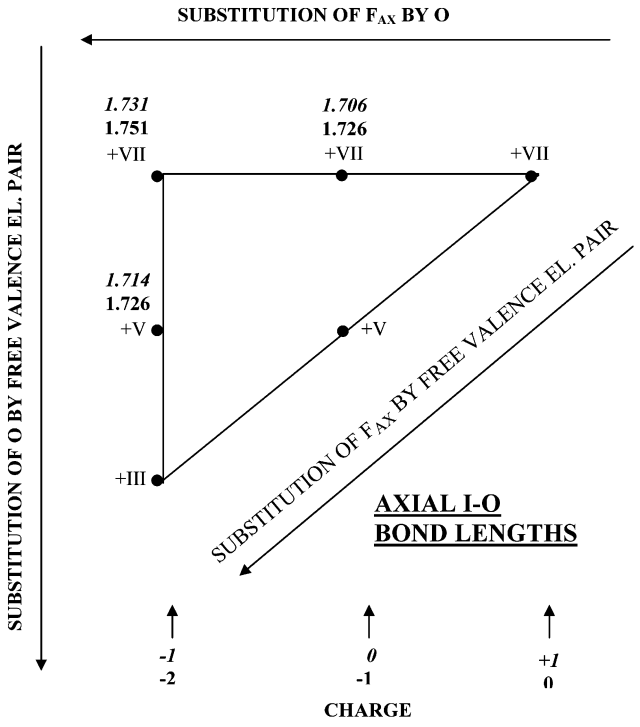

Figure 8. Changes of the axial I−O bond lengths (Å) with increasing ion charge and decreasing oxidation state of the central iodine atom. Italic and nonitalic numerals represent the hexa- and heptacoordinated species, respectively.

exhibit the shortest I−F bonds (1.75 Å), while IF_5^{2-}, with two negative ion charges, an iodine oxidation state of III, a CN of 7, and two free iodine valence electron pairs, has the longest I−F bonds of 2.095 Å. This wide range in the I−F bond lengths is quite remarkable.

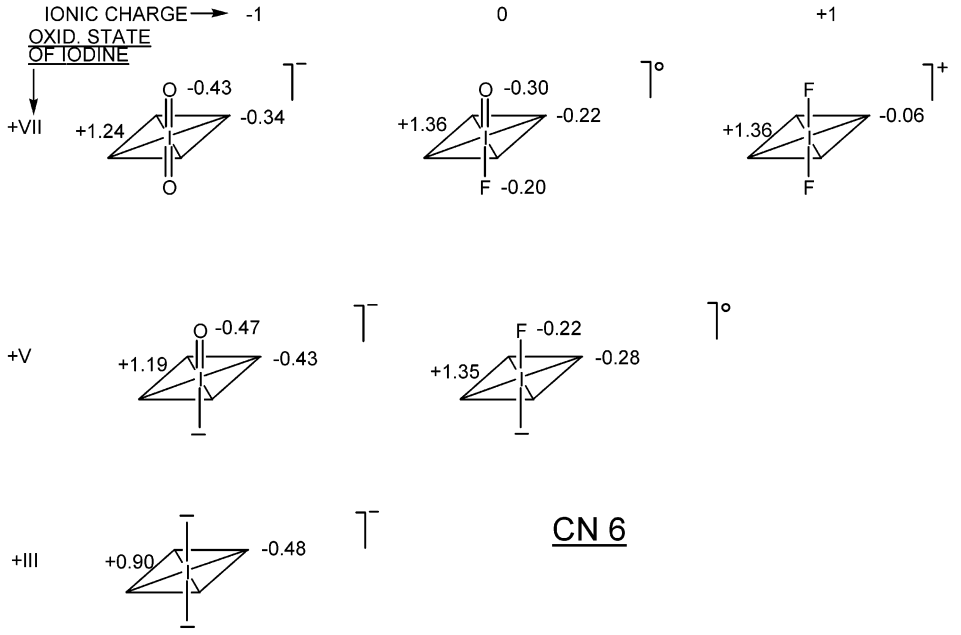

Figure 9. Mulliken charges for the hexacoordinated $IO_2F_4^-$, IOF_4^-, IF_4^-,IOF_5, IF_5, and IF_6^+ ions and molecules, calculated in this study at the HF/ECP/DZVP level of theory.

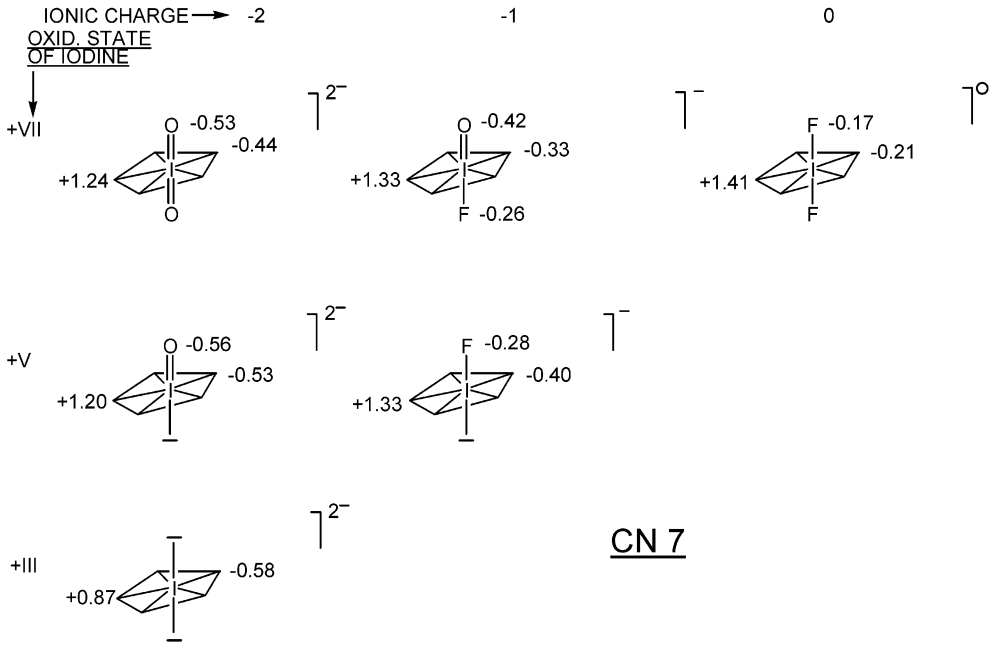

Figure 10. Mulliken charges for the heptacoordinated $IO_2F_5^{2-}$, IOF_5^{2-}, IF_5^{2-}, IOF_6^-, IF_6^-, and IF_7 ions and molecules, calculated in this study at the HF/ECP/DZVP level of theory.

(vi) The O−I−F bond angles in IOF_4^- and IOF_5^{2-}, which contain one oxygen atom and one free valence electron pair in the two axial positions, provide information concerning the relative repulsion domains of doubly bonded oxygen and a sterically active free valence electron pair. In both ions, the O−I−F angle is somewhat larger than 90°, indicating that, in these compounds, the doubly bonded oxygen domain is slightly more repulsive than that of the free valence electron pair.

(vii) The toal charge distributions (Mulliken charges) are given in Figures 9 and 10. It can be seen that the negative charges are located on the ligands because of their higher electronegativities and increase, as expected, with increasing ion charges and decreasing oxidation state of the central atom. The central atoms carry large positive charges, and their values also decrease with increasing ion charges and decreasing oxidation state.

(viii) The experimentally observed bond distances (see Figures 3 and 4) are in accord with the calculated trends except for the axial I−F bond reported for IOF_5.[45] The reported electron diffraction data did not permit an unambiguous determination of this distance, and a redetermina-

(45) Bartell, L. S.; Clippard, F. B.; Jacob, E. J. *Inorg. Chem.* **1976**, *15*, 3009.

tion of this structure by X-ray crystallography or other methods is called for. In accord with a previous study,[11] we predict that the axial I−F bond length is 1.815 Å, close to that of the equatorial I−F bonds.

(ix) The previously proposed bonding models[3,9] are consistent with the structures observed for these iodine fluorides and oxide fluorides. On the basis of these models, the oxygen−iodine σ-bonds and the free valence electron pairs of iodine seek high s character by utilizing sp^n orbitals of the iodine atom, while the remaining fluorine ligands are relegated to form with the remaining p orbitals highly ionic, multicenter bonds.[3,9,42−44]

Conclusions

The fluoride ion acceptor properties of *cis*-$IO_2F_4^-$ and *trans*-$IO_2F_4^-$ have been studied. Because of an expected large activation energy barrier in a *cis*-$IO_2F_4^-/F^-$ adduct toward rearrangement to the energetically favored D_{5h} *trans*-$IO_2F_5^{2-}$ structure, only the *trans*-$IO_2F_4^-$ anion acts as a fluoride ion acceptor. The resulting novel *trans*-$IO_2F_5^{2-}$ anion has been isolated and characterized and is presently the only known main-group $AO_2F_5^{n-}$ species. On the basis of its vibrational spectra and electronic structure calculations, the $IO_2F_5^{2-}$ anion has the pentagonal-bipyramidal geometry preferred by main-group fluorides and oxide fluorides with CN 7. An analysis of the calculated structures of six- and seven-coordinate iodine fluorides and oxide fluorides reveals systematic trends that are dominated by changes in the ionicity of the I−F bonds because of the formal ionic charges of the species and the oxidation states of the central atom.

Acknowledgment. We thank the donors of the Petroleum Research Fund, administered by the American Chemical Society, for support of this work under ACS-PRF No. 37128-AC3 (G.J.S.) and the Ontario Ministry of Education and the Richard Fuller and James A. Morrison Memorial Funds, McMaster University, for the award of graduate scholarships (M.G.). The work at USC was financially supported by the National Science Foundation, and that at Edwards, by the Air Force Office of Scientifc Research and the Defense Advanced Research Projects Agency. A part of this work at the Pacific Northwest Laboratory was supported by the Department of Energy. We thank Dr. Ross Wagner for his help with the preparation of some starting materials, Dr. Robert Syvret for his preparation of the IO_2F_3 sample, and Dr. William J. Casteel, Jr., for some exploratory experiments involving IO_2F_3 and $[N(CH_3)_4][F]$.

IC034457W